Microstructure and compressive properties of porous hybrid materials consisting of ductile Al/Ti and brittle Al_3Ti phases fabricated by reaction sintering with space holder.

Asuka Suzuki[a,*], Naoki Kosugi[b], Naoki Takata[a], Makoto Kobashi[a]

[a]Department of Materials Process Engineering, Graduate School of Engineering, Nagoya University, Furo-cho, Chikusa-ku, Nagoya, 464-8603 Japan

[b]Department of Materials Science and Engineering, Graduate School of Engineering, Nagoya University, Furo-cho, Chikusa-ku, Nagoya, 464-8603 Japan

* Corresponding author,

Asuka Suzuki

E-mail address: suzuki.asuka@material.nagoya-u.ac.jp

Abstract

The strain-hardening of cell wall in porous metals decreases the energy absorption properties. In order to suppress the strain hardening, porous hybrid materials consisting of ductile Al and Ti phases and brittle Al_3Ti phase were synthesized by reaction sintering between Al and Ti powders with NaCl space holder. Changes in the porous structure and microstructure with sintering were investigated. Area fraction of Al_3Ti phase formed at Al/Ti interface increased following the Johnson-Mehl-Avrami-Koromogrov (JMAK) equation of three-dimensional diffusion-controlled growth with zero nucleation rate. The growth of Al_3Ti phase led to the formation of pores and cracks in cell wall by Kirkendall effect and volume shrinkage. Effect of microstructure on compressive properties of the porous Al/Al_3Ti/Ti hybrids were also investigated. Porous hybrids consisting of α-Al matrix exhibited the plateau region with positive slopes due to the strain hardening of α-Al phase. Porous hybrids consisting of Al_3Ti matrix exhibited the plateau region with the slope of almost zero, resulting in high energy absorption capacity and efficiency. Fractography revealed that crack propagated in brittle Al_3Ti phase but arrested at α-Al phase. These results were used to discuss the microstructure for improving energy absorption properties.

Keywords:

Porous metals; Energy absorption; Reaction sintering; Space holder method; ductile/brittle phases hybrid; Titanium aluminide

1. Introduction

Porous metals exhibit unique properties like ultra-low weight, high specific stiffness, low thermal conductivity, and impact energy absorptivity [1]. For example, porous metals can absorb large impact energy under almost constant load, which appears as the plateau region in the stress-strain curves. According to International Organization for Standardization (ISO) [2], the energy absorption capacity (W) and efficiency (η) of porous metals are defined as follows.

$$W = \int_0^{\varepsilon_{\mathrm{end}}} \sigma d\varepsilon , \tag{1}$$

$$\eta = \frac{W}{1.3\sigma_{\mathrm{pl}} \cdot \varepsilon_{\mathrm{end}}} , \tag{2}$$

where σ and ε are the compressive stress and strain, σ_{pl} is the plateau stress, and $\varepsilon_{\mathrm{end}}$ is the plateau end strain. The plateau stress is defined as the average flow stress in a nominal strain range of 20-30%. The plateau end strain is defined as the strain at which the flow stress reaches 1.3 times the plateau stress. Energy absorption capacity increases with increasing the plateau stress. However, the plateau stress is required not to exceed the load capacity of components protected by the energy absorber [3]. Larger plateau end strain is the most effective for higher energy absorption capacity. High energy absorption capacity and efficiency can be also achieved by making the slope in the plateau region as close to zero as possible. However, most of the porous metals exhibit the plateau region with positive slopes [4, 5]. This is because the cell wall consisting of ductile metals are strain-hardened by the bending deformation of during compression. Recently, it is reported that porous metals consisting of brittle intermetallic compounds exhibit flat plateau region with large plateau end strain [6-8].

The processes used to fabricate the porous metals include continuous casting [9, 10],

slurry processing [11, 12], space holder method [13], foaming using a gas blowing agent [14,15], and combustion synthesis foaming [16,17]. The space holder method forms pores by removing space holder particles added in sintered or cast materials. This method permits controlling porosity, pore size, and pore morphology precisely. For example, porous aluminum (Al) is fabricated using sodium chloride (NaCl) space holder particles [13] because NaCl is chemically stable in Al and has a higher melting point (800 ºC) than Al (660 ºC). The porous intermetallic compounds can be fabricated by combining the space holder method with combustion reaction. The combustion reaction can synthesize ceramics and intermetallic compounds with high melting points instantly by generating a large amount of heat [18-20]. Kobashi et al. and Jiao et al. successfully fabricated TiAl intermetallic compounds with a hierarchical open-cell structure by the combustion synthesis reaction between Al and Ti powders and the space holder method using NaCl particles [21, 22]. It is reported that the combustion reaction proceeds gradually when induced in the spark plasma sintering (SPS) apparatus [23, 24]. Therefore, the spark plasma reaction sintering permit controlling the amount of the intermetallic compounds by the sintering condition.

In the present study, effects of sintering temperature and time on porous structure and microstructure of porous Al/Al_3Ti/Ti hybrids with interfacial Al_3Ti phase synthesized by the spark plasma reaction sintering with NaCl space holder was investigated. Changes in the energy absorption properties with synthesis of Al_3Ti phase were also studied to obtain a concept for fabricating porous metals with a flat and wide plateau region.

2. Experimental procedure

Al powders (purity: 99.99%, average size: 20 μm), Ti powders (purity: 99%, size: <

38 μm), and NaCl space-holder powders (purity: 95.0%, size: 330–430 μm) were used. The morphology of these powders is shown in Fig. 1 (a-c). The Al and Ti powders were blended in an atomic ratio of 3:1. In view of the equilibrium phase diagram for Al-Ti binary system [25], a single-phase of Al_3Ti intermetallic compound with a $D0_{22}$ crystal structure are present in the equilibrium condition. The space-holder NaCl powders were blended with the Al-Ti powder mixture so that the volume fractions of NaCl were 70%. The strain hardening becomes more significant as the porosity decreases. So, minimum volume fraction of NaCl which can be leached away [26] was selected. The powder mixture was placed in a graphite mold (inner diameter: 20 mm, outer dimeter: 40 mm, and height: 50 mm) and sintered in a SPS apparatus in vacuum (<10 Pa) while applying a constant pressure (20 MPa). The schematic illustration of the SPS apparatus is shown in Fig. 2. The temperature of the surface on the graphite mold was measured by a radiation thermometer. The temperature was increased at a rate of 0.5 ℃/s and held at 600 ℃ and 620 ℃ for 0-3600 s. These temperatures were selected in view of balance between temperatures below the melting point of Al (660 °C) and higher reaction rate. Subsequently, the samples were furnace cooled to ambient temperature. The appearance of a representative sintered sample is shown in Fig. 1 (d). The sample had a dimeter of 20 mm and a height of 15 mm. The samples were soaked in pure water for 86.4 ks to remove the NaCl space holder. The porosity derived from the NaCl space holder was calculated by the mass of the sample before and after soaking and the sample size.

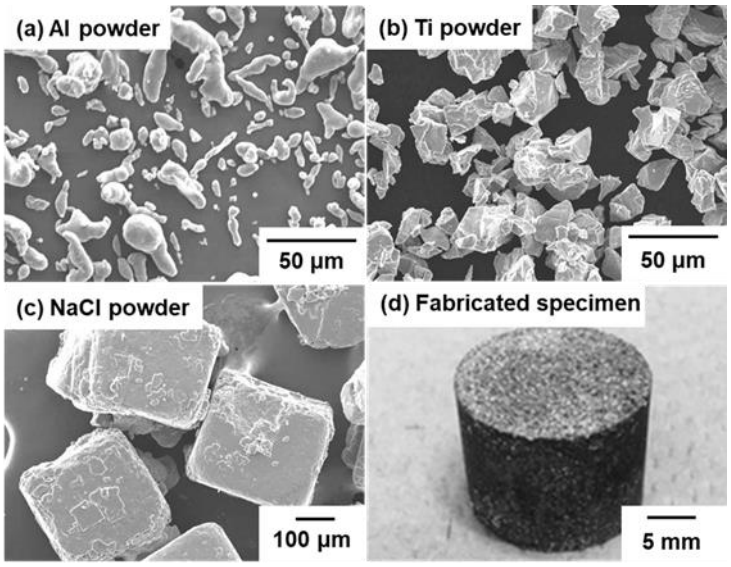

Fig. 1 (a-c) Secondary electron images (SEIs) showing morphology of the raw powders used in this study: (a) Al, (b) Ti, and (c) NaCl. (d) Photograph showing appearance of the porous Al/Ti composite fabricated in this study.

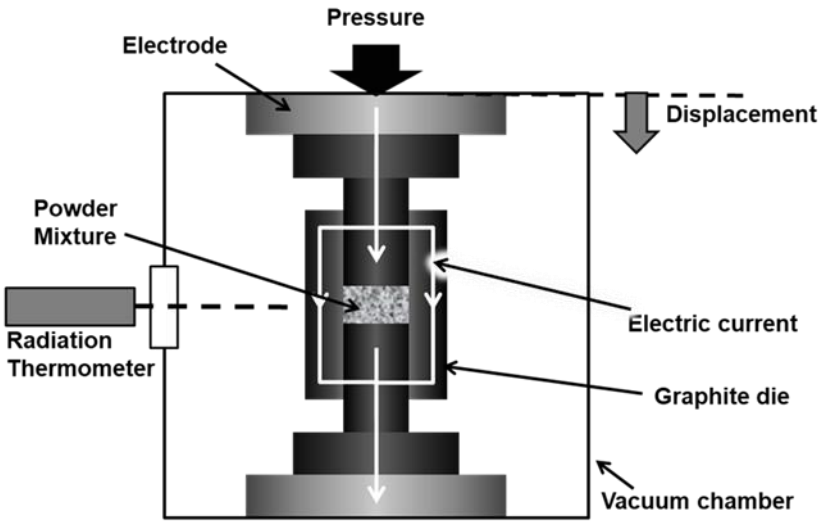

Fig. 2 Schematic illustration showing the spark plasma sintering (SPS) apparatus used in this study.

The samples were soaked in an uncured epoxy resin and the resin was cured. After curing, the samples were polished using SiC abrasive papers (#120, 320, 800, 1200, and 2400) and diamond slurries of 9 μm, 3 μm, and 1 μm. The porous structure and

microstructure were observed using a JSM-6610A scanning electron microscope (SEM) operating at 25 kV. Area fractions of the Al_3Ti phase and pores were quantified by the image analysis. The chemical compositions were analyzed with energy dispersive X-ray spectroscopy (EDS) at 25 kV. The constituting phases of the samples were analyzed using an X-ray diffraction (XRD) system operating at 40 kV and 40 mA with a Cu-Kα radiation source.

The compressive tests were performed at a strain rate of approximately 4.4×10^{-3} s^{-1} at room temperature. The energy absorption capacity and efficiency were calculated from the compressive-strain curves. In the present study, the plateau region was defined as the nominal strain range from 10-20%. This is because, in the range of nominal strains of 20-30% of the ISO standard, some of the samples were already in a densified region where the stresses increased.

3. Results

Figure 2 presents backscattered electron images (BEIs) showing the porous structure in the porous hybrid materials sintered at (a, b) 600 ºC and (c, d) 620 ºC for (a, c) 0 s and (b, d) 2400 s. The darkest contrast shows pores derived from the NaCl space holder powder. The pores replicated morphology of a cuboidal shape of the NaCl particles shown in Fig. 1 (c). Figure 2 shows the change in the porosity derived from the NaCl particles as a function of the sintering time. The porosity was almost constant at approximately 70%, which was the volume fraction of NaCl in the raw powder mixture. It was confirmed that the sintering temperature and time did not affect the porous structure formed by the NaCl particles.

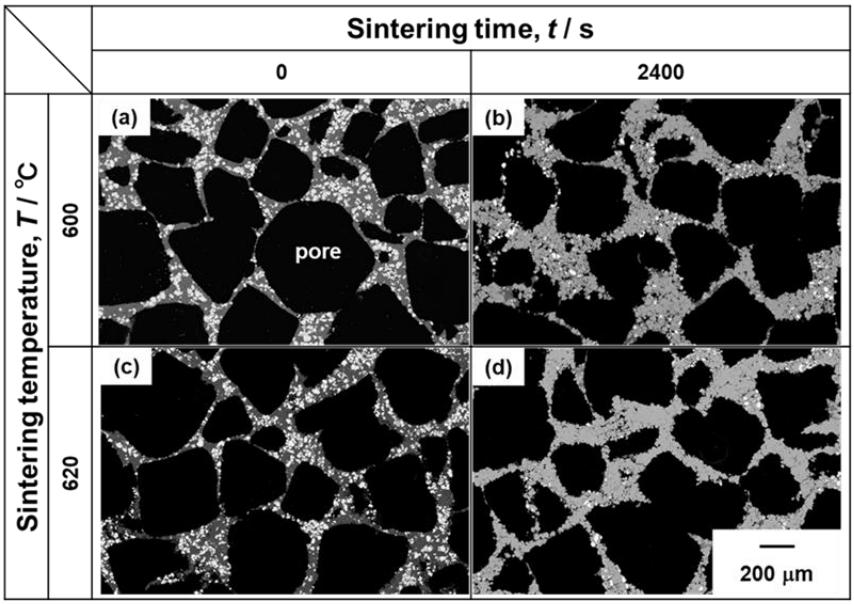

Fig. 4 Low-magnification backscattered electron images (BEIs) showing porous structure in the porous hybrid materials sintered at (a, b) 600 ºC and (c, d) 620 ºC for (a, c) 0 s and (b, d) 2400 s.

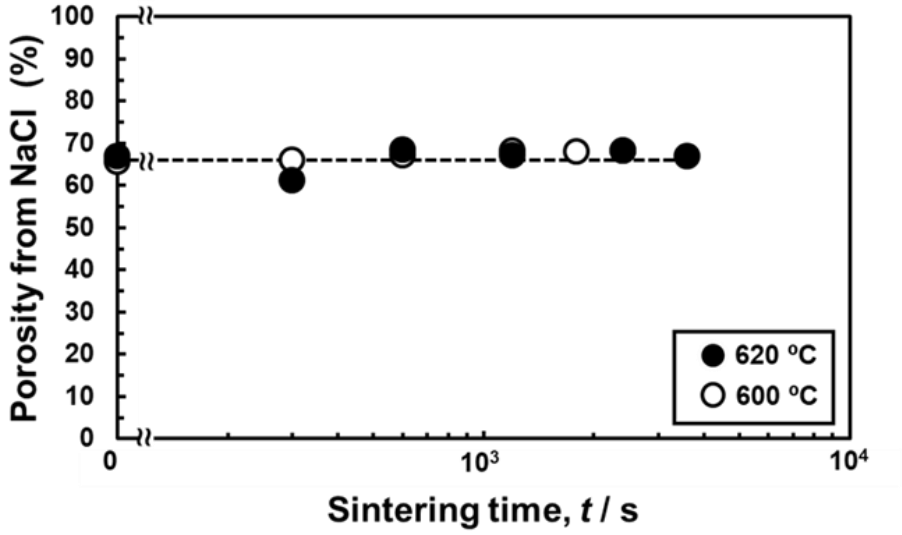

Fig. 4 Change in the porosity derived from NaCl space holder particles as a function of the sintering time.

Figure 5 presents the XRD profiles of the porous hybrid materials sintered at (a, b) 600 ºC and (c, d) 620 ºC for (a, c) 300 s and (b, d) 2400 s. The constituent phases were α-Al (fcc), α-Ti (hcp), and Al_3Ti ($D0_{22}$). Other intermetallic phases such as TiAl and

Ti_3Al did not form. Figure 6 present BEIs showing microstructure in the cell wall of porous Al/Al_3Ti/Ti hybrids sintered at (a-d) 600 ºC and (e-h) 620 ºC for (a, e) 0 s, (b, f) 300 s, (c, g)1200 s, and (d, h) 2400 s. At 0 s, α-Ti phases with the brightest contrast maintained the original shape of Ti powder particles shown in Fig. 1 (b) and surrounded by dense α-Al phase (Fig. 6 (a, e)). The Al_3Ti phase formed at the interface between α-Al and α-Ti phases and grew as the sintering proceeded (Fig. 6 (b-d, e-g)). The higher sintering temperature was, the faster the Al_3Ti phase grew (Fig. 6 (b, c, f, g)). As the growth of Al_3Ti phase progressed, pores and cracks with the darkest contrast were formed in the cell wall (Fig. 6 (c, d, g, h)). Figure 7 shows (a) high-magnification BEI, (b) EDS element maps of Al and Ti of the porous Al/Al_3Ti/Ti hybrid sintered at 600 ºC for 300 s and (c) results of EDS quantitative analysis at the points shown in (a). In the Al-Ti intermetallic compound with middle contrast, Al and Ti are were detected at a molar ratio of approximately 3:1. Comparing the results with XRD results shown in Fig. 5, it was confirmed that the Al-Ti intermetallic compounds was Al_3Ti phase. Al and Ti were slightly detected in α-Ti and α-Al phases, respectively, which was an indicator of interdiffusion of these elements.

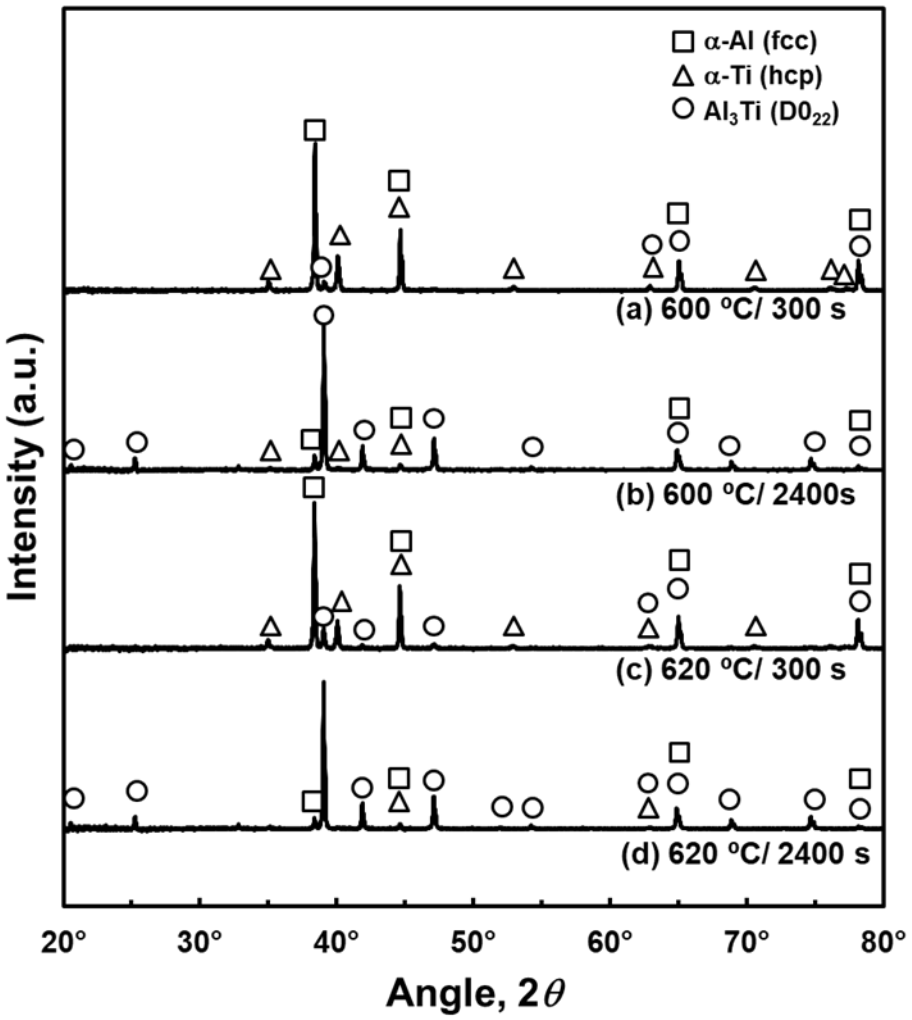

Fig. 5 XRD profiles of the porous hybrid materials sintered at (a, b) 600 ºC and (c, d) 620 ºC for (a, c) 300 s and (b, d) 2400 s.

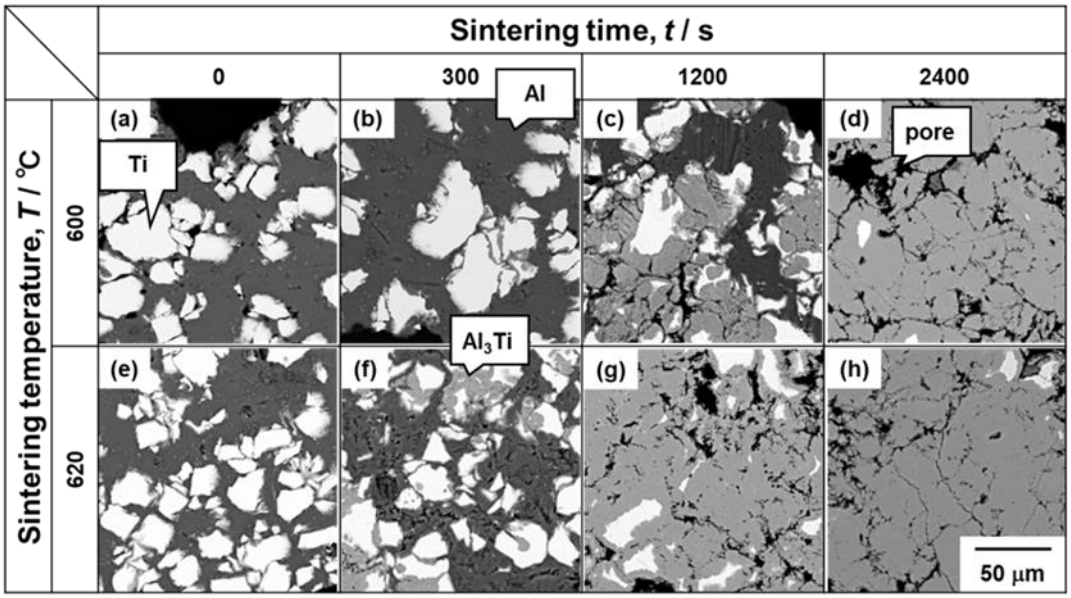

Fig. 6 High-magnification BEIs showing microstructure in cell wall of the porous Al/Al_3Ti/Ti hybrids sintered at (a-d) 600ºC and (e-f) 620 ºC for (a, e) 0 s, (b, f) 300 s, (c, g) 1200 s, and (d, h) 2400 s.

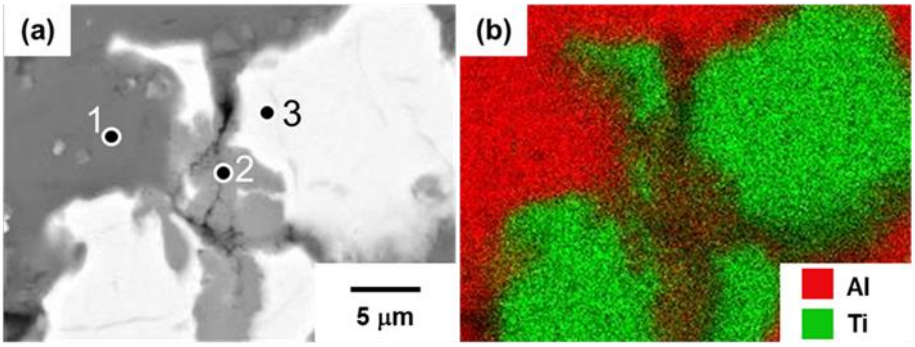

(c)

point	Concentration (mol%)	
	Al	Ti
1	99.3	0.7
2	74.1	25.9
3	1.6	98.4

Fig. 7 (a) High-magnification BEIs and (b) EDS element map of Al and Ti in the porous Al/Al_3Ti/Ti hybrid sintered at 600ºC for 300 s and (c) results of EDS quantitative analysis of Al and Ti at the points shown in (a).

Figure 9 presents changes in (a) the area fraction of Al_3Ti phase (A_{Al_3Ti},) (b) -ln (1-A_{Al_3Ti}), and (c) the porosity in cell wall in the porous Al/Al_3Ti/Ti hybrids as a function of the sintering time. Note that the porosity does not include pores derived from the NaCl particles and is the volume fraction of pores and cracks occupying the cell wall. The area fraction of Al_3Ti phase increased to approximately 100% (equilibrium condition) with S-curves (Fig. 9). The growth rate of Al_3Ti phase at 620 ºC was faster than that at 600 ºC. The data points were regressed with the following Johnson-Mehl-Avrami-Koromogrov (JMAK) equation [27-30].

$$A_{Al_3Ti} = 1 - \exp(-kt^n), \quad (3)$$

where k is the temperature-dependent rate constant and n is the temperature-independent exponent. The exponent was obtained from the slope of regression lines of the correlation between -ln(1-A_{Al_3Ti}) and the sintering time shown in Fig. 9 (b). The exponent was approximately 1.5 regardless of the sintering temperature. The rate constants (k) were 1.6×10^{-5} $s^{-1.5}$ at 600 ºC and 4.8×10^{-5} $s^{-1.5}$ at 620 ºC. The porosity in cell wall also increased to approximately 13% with S-curves as shown in Fig. 9 (c). The porosity increased at 620 ºC faster than at 600 ºC. The change tendency of the porosity was similar to that of the area fraction of Al_3Ti phase. The formation of pores is related to the formation of Al_3Ti phase.

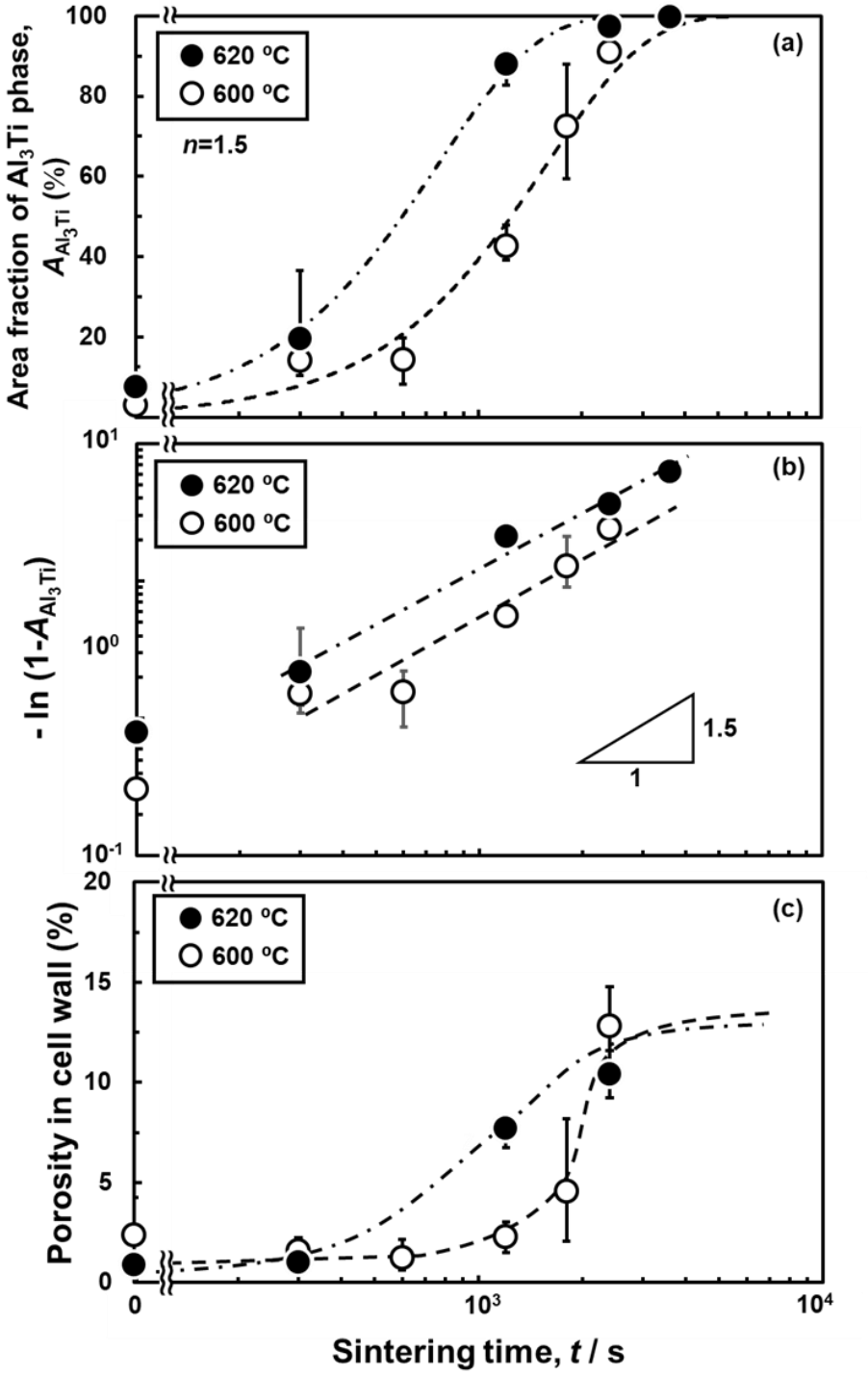

Fig. 8 Changes in (a) the area fraction of Al_3Ti phase (A_{Al_3Ti},) (a) -ln (1-A_{Al_3Ti}), and (c) the porosity in cell wall in the porous Al/Al_3Ti/Ti hybrids as a function of the sintering time.

Figure 9 presents the compressive-stress strain curves of porous Al and Al/Al_3Ti/Ti hybrids sintered at 600 ºC for 0, 600, 1200, 1800 s, and 2400 s. The porous Al exhibited the plateau region with positive slopes. The plateau stress and end strain were approximately 10 MPa and 40%. The stress-strain curves had slopes in the plateau region also in the case of porous Al/Al_3Ti/Ti hybrids sintered for 0-1200 s. The plateau stresses and the plateau end strains were in the range of 10-15 MPa and 20-40%. When the sintering time was in 1800 s, the plateau region was almost flat. The plateau region was enlarged to approximately 60% although the plateau stress was slightly decreased to approximately 10 MPa. When the specimen was sintered for 2400 s, the flow stress decreased gradually in the plateau region although the plateau end strain further increased to approximately 75%. Figure 10 presents changes in the energy absorption capacity and efficiency evaluated from Fig. 9 as a function of the sintering time. The values of porous Al were shown by the gray arrows. Both the energy absorption capacity and efficiency increased with increasing the sintering time until 1800 s and decreased when the sintering time was 2400 s. The porous Al/Al_3Ti/Ti hybrids sintered for 1800 s exhibited both higher energy absorption capacity and efficiency than porous Al. The increment in the energy absorption properties until 1800 s was due to the flattening and enlargement of the plateau region. In contrast, the decrement in the energy absorption properties at 2400 s was caused by the decrease in the flow stress in the plateau region.

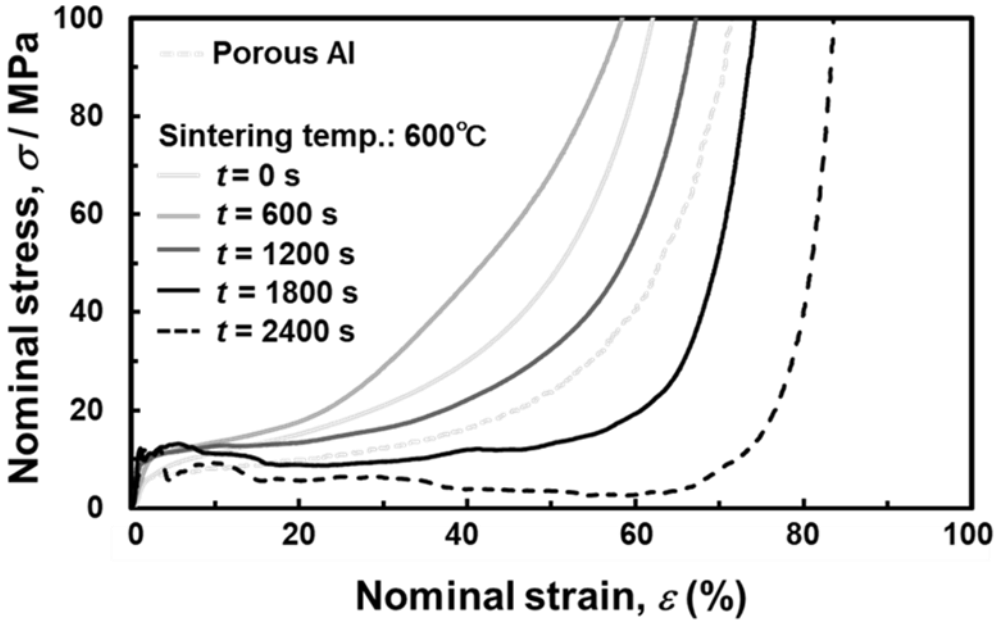

Fig. 9 Nominal stress-strain curves of the porous Al/Al_3Ti/Ti hybrids sintered at 600℃ for 0, 600, 1200, 1800, and 2400 s. The stress-strain curve of porous Al was also shown in the figure.

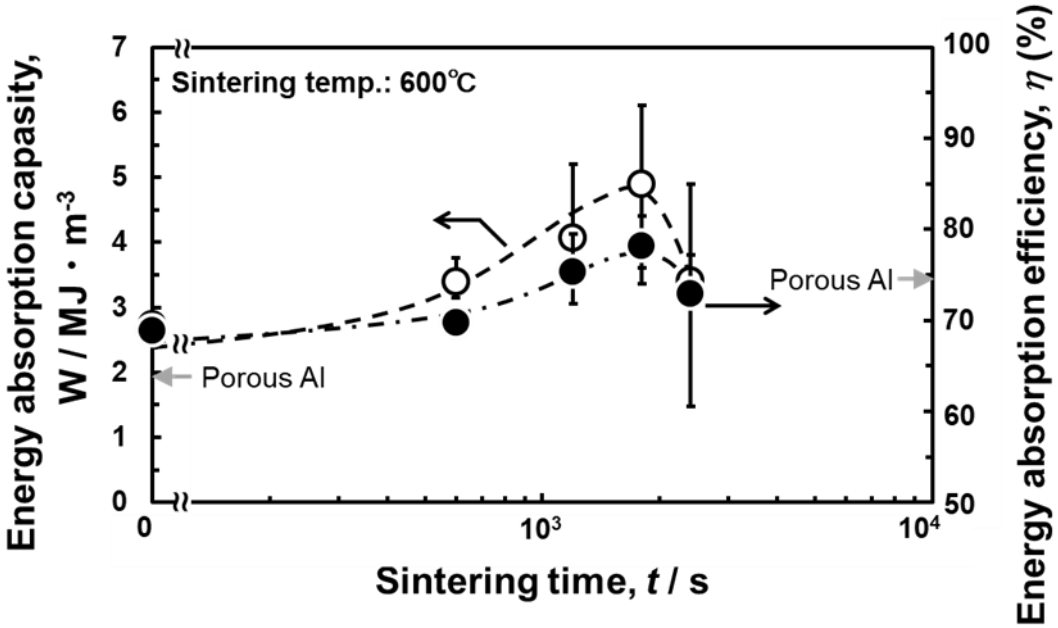

Fig. 10 Changes in the energy absorption capacity and energy absorption efficiency as a function of the sintering time at 600 ºC. The values of porous Al were also shown by gray arrows.

The energy absorption capacity and efficiency of the porous Al/Al_3Ti/Ti hybrid sintered at 600°C for 1800 s were plotted as a function of the bulk density in Fig. 11 to compare with results of other porous materials [4,5,7,31,32] fabricated by space holder method. Porous Al and Ti exhibit high energy absorption capacity (Fig. 11 (a)) but relatively low efficiency (Fig. 11 (b)). On the other hand, porous NiAl, which is a brittle intermetallic-based porous material, exhibit high energy absorption efficiency (Fig. 11 (b)) but low capacity (Fig. 11 (a)). The energy absorption capacity of the porous Al/Al_3Ti/Ti hybrid was almost the same level of the porous Ti and higher than porous Al and NiAl (Fig. 11 (a)). The energy absorption efficiency of the porous Al/Al_3Ti/Ti hybrid was higher than that of porous Ti and Al, and roughly the same level of the porous NiAl (Fig. 11 (a)). Thus, the porous Al/Al_3Ti/Ti hybrid exhibited both high energy absorption capacity and efficiency.

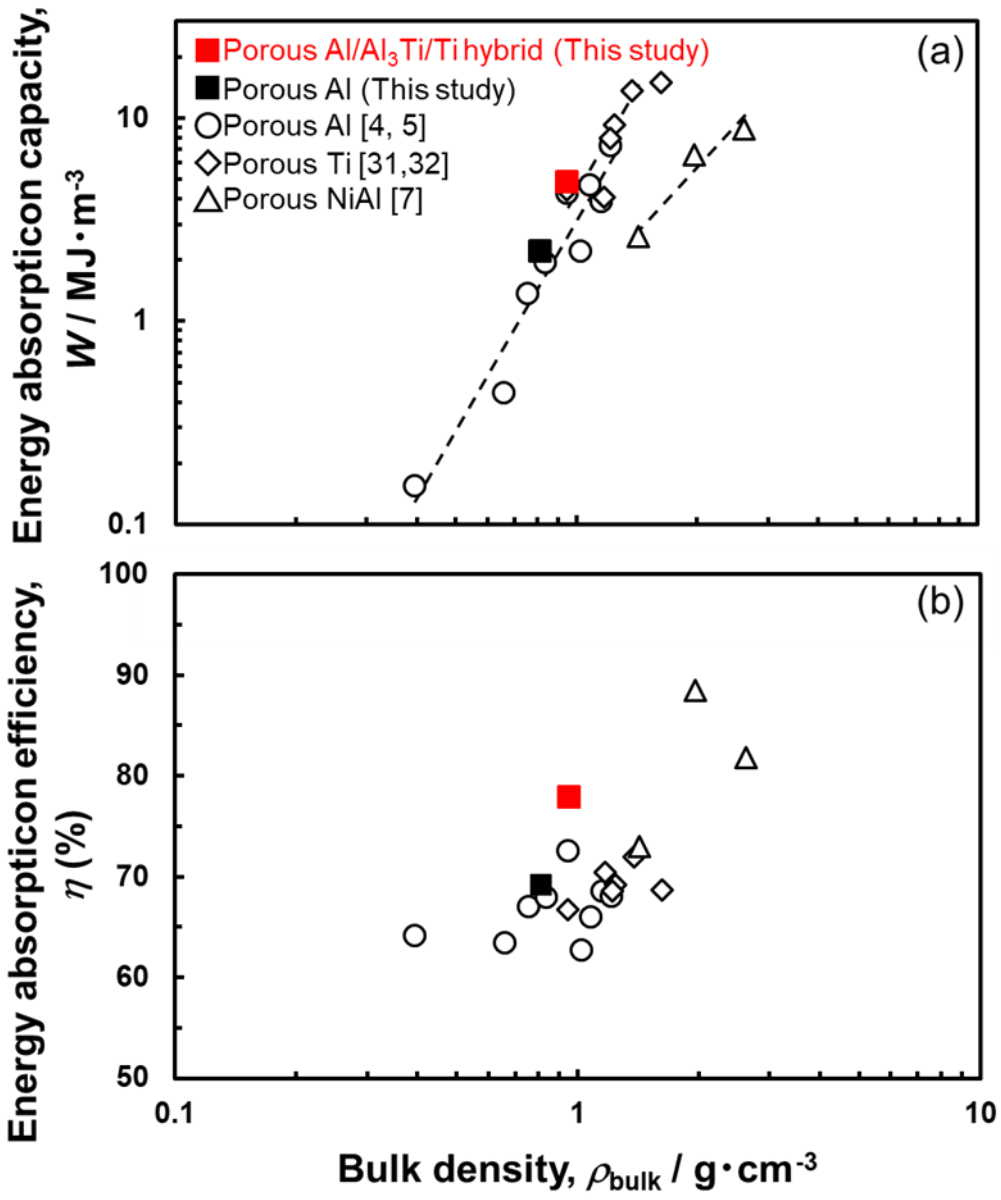

Fig. 11 Changes in the energy absorption capacity and energy absorption efficiency as a function of bulk density. For comparison, results of other porous materials were also plotted.

Figure 12 present compressive deformation behaviors at nominal strains of (a-c) 30%, (d-f) 50% of porous Al/Al_3Ti/Ti hybrids sintered at 600ºC for (a, d) 1200 s, (b, e) 1800 s, and (c, f) 2400 s. The porous specimen sintered for 1200 s deformed in a barrel shape (Fig. 12 (a, d)). In contrast, the porous specimen sintered for 2400 s exhibited surface cracks when the nominal strain was 30% (Fig. 12 (c)) and deformed while collapsing (Fig. 12 (f)). No millimeter-sized cracks were observed on the surface of the specimen sintered for 1800 s during the compression tests (Fig. 12 (b, e)).

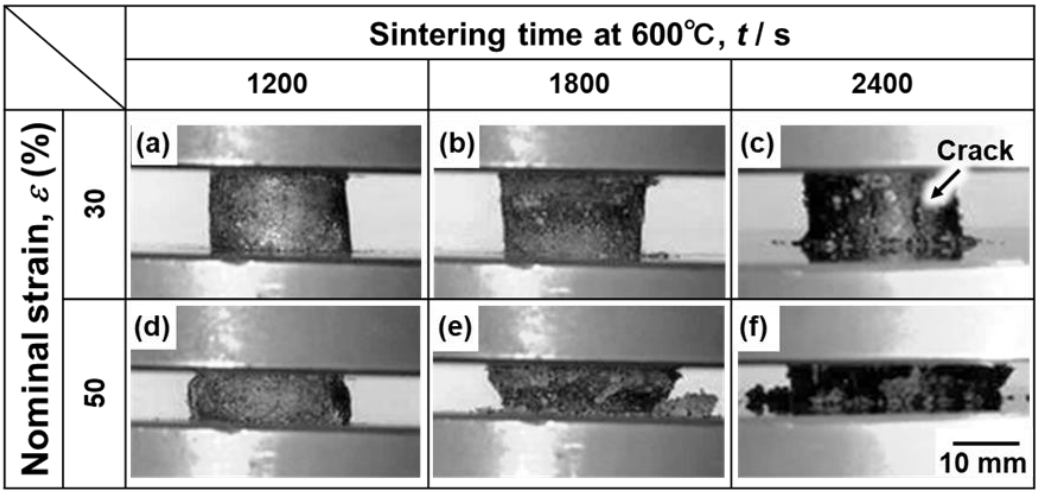

Fig. 12 Compressive deformation behaviors at nominal strains of (a-c) 30%, (d-f) 50% of the porous Al/Al_3Ti/Ti hybrids sintered at 600ºC for (a, d) 1200 s, (b, e) 1800 s, and (c, f) 2400 s.

4. Discussion

In the present study, effects of sintering temperature and time on porous structure, microstructure, and compressive properties were investigated. The area fraction of Al_3Ti phase increased following the JMAK equation (Fig. 8 (a)) with an exponent (n) of 1.5 (Fig. 8 (b)). The porosity in cell wall increased with increasing the area fraction of Al_3Ti phase (Fig. 8 (c)). It is known that a value of n = 2.5 represents a three-dimensional

diffusion-controlled growth with a constant nucleation rate during the growth process, and a value of n = 1.5 represents the growth with zero nucleation rate [29]. In the process in this study, Al_3Ti phase formed preferentially at the interface between Al and Ti phases. Once Al_3Ti phase forms at the interface, it grows by the solid-solid reactions among Al, Al_3Ti, and Ti phases. The growth does not involve the formation of new nuclei, resulting in the growth with an exponent of 1.5. Previous studies revealed that the growth of Al_3Ti phase caused by the solid-solid reaction is limited by the atomic diffusion of Al in Al_3Ti phase [33-35]. The Kirkendall voids are formed where Al particles originally existed [36]. In addition, the formation and growth of Al_3Ti phase from α-Al and α-Ti phases lead to volume shrink. The average volume per one atom of α-Al, α-Ti, and Al_3Ti phases are 16.6, 17.6, and 15.9 $Å^3$. The reaction of $3Al+Ti \rightarrow Al_3Ti$ shrinks the volume 5.4%, resulting in the formation of pores and cracks. Therefore, the porosity in cell wall increases with increasing the area fraction of Al_3Ti phase.

It is also interesting that the porous Al/Al_3Ti/Ti hybrid sintered at 600 ºC for 1800 s exhibited a flat plateau region with a large plateau end strain (Fig. 9), resulting in both higher energy absorption capacity and efficiency (Fig. 11, 12). The porous structure derived from the NaCl particles did not change depending on the sintering conditions (Fig. 3, 4). Therefore, it is considered that porous structure and microstructure in the cell wall affected the change in the compressive properties of the porous Al/Al_3Ti/Ti hybrids. Figure 13 presents (a, b) Low- and (c, d) High-magnification BEIs showing microstructure of the porous Al/Al_3Ti/Ti hybrids sintered at 600 ºC for (a, c) 600 s and (b, d) 1800 s and subsequently compressed to a nominal strain of 30%. The cell wall of the porous Al/Al_3Ti/Ti hybrid sintered at 600 ºC for 600 s deforms in a bending manner

(Fig. 13 (a, c)). The area fraction of Al_3Ti phase in the specimen was approximately 15% (Fig. 10 (a)). The cell wall exhibited the ductile deformation since the matrix of the specimen was α-Al phase. In contrast, as shown in Fig. 13 (b, d), cracks were propagated in Al_3Ti phase in cell wall of the porous Al/Al_3Ti/Ti hybrid. The crack propagation seems to be caused by connections of the pores and cracks formed by reaction sintering. The area fraction of the sample was approximately 70% (Fig. 8 (a)), and the matrix was Al_3Ti phase instead of α-Al phase. It is reported that polycrystalline Al_3Ti phase does not exhibit plastic deformability at room temperature [37]. The brittleness of Al_3Ti suppressed the strain hardening of cell wall. However, the flow stress of the porous Al/Al_3Ti/Ti hybrid sintered at 600 ºC for 2400 s ($A_{Al_3Ti} \approx 90\%$) decreased gradually in the plateau region (Fig. 9). Therefore, α-Al phase also played a role in exhibiting a flat plateau region. As shown in Fig. 13 (d), cracks stopped at α-Al phase (white circle in the figure). The ductility of α-Al phase arrested the crack propagation and suppress the surface crack shown in Fig. 12 (c), resulting in flat plateau region.

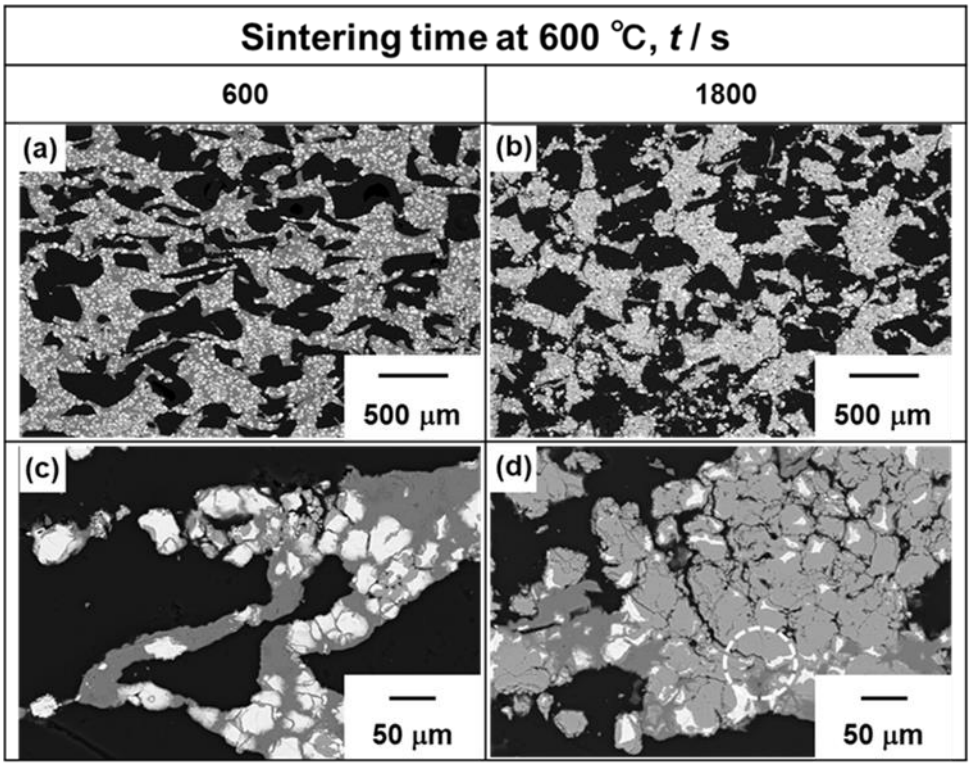

Fig. 13 (a, b) Low- and (c, d) High-magnification BEIs showing the microstructure of the porous Al/Al_3Ti/Ti hybrids sintered at 600 ºC for (a, c) 600 s and (b, d) 1800 s and subsequently compressed to a nominal strain of 20%.

When the area fraction of Al_3Ti is around 70%, it is thought that Al_3Ti phase is the matrix (continuous) and Al phase remains the most. Here, the area fraction of Al_3Ti for obtaining Al_3Ti matrix will be discussed below. Figure 14 (a) presents schematic illustration of a cross-section of Al/Ti compact before Al_3Ti phase forms (Fig. 6). Ti particles with various sizes and shapes are randomly distributed in α-Al matrix. For simplicity, it is assumed that Ti particles have a spherical shape with uniform size (average size on a cross-section) and arranged in at equal intervals (Fig. 14 (b)). In this case, the interval (L) is expressed in the following equation.

$$L = \left(\frac{1}{2} \sqrt{\frac{\pi}{A_{\mathrm{Ti}}}} - 1 \right) \bar{d}_{\mathrm{Ti}}, \tag{4}$$

where A_{Ti} is the area fraction of Ti particles, which is 0.26 in this study, and $\bar{d}_{Ti}$ is the average size of Ti particles on a cross-section. Assuming that Al_3Ti forms and grows isotopically around Ti particles (Fig. 14 (c)), the diameter of Al_3Ti+unreacted Ti needs to be $\bar{d}_{Ti}+L$. Considering the stoichiometric ratio of the reaction ($3Al+Ti \rightarrow Al_3Ti$) and the molar volumes of each phase, the minimum area fraction of Al_3Ti phase for obtaining Al_3Ti matrix material is estimated to be approximately 71%, which is in good agreement of the area fraction of Al_3Ti phase of the sample with the highest energy absorption capacity and efficiency in this study (approximately 70%). In order to enhance the energy absorption capacity and efficiency, it is important that the brittle intermetallic compounds are used as the matrix while the ductile phases remain as much as possible.

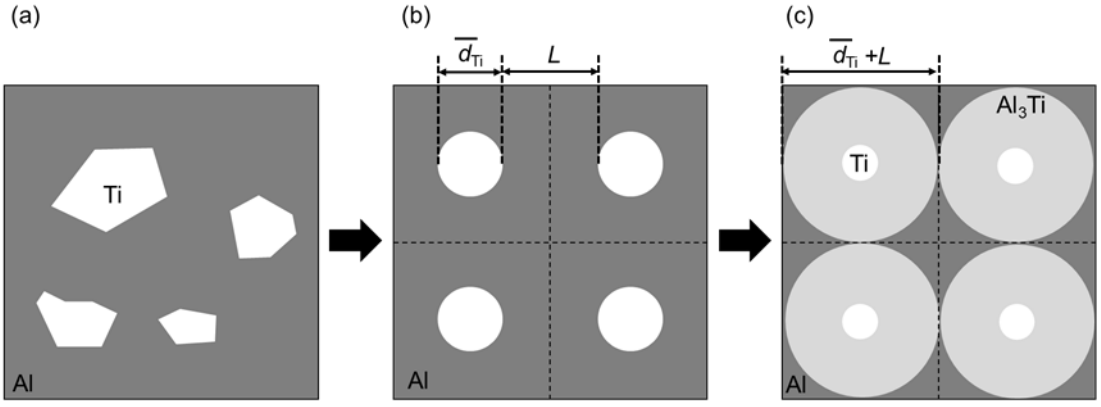

Fig. 14 Schematic illustrations of (a) a cross-section in Al/Ti compact before Al_3Ti forms, (b) model in which spherical Ti particles with uniform size are arranged at equal intervals, and (c) model with the minimum area fraction of Al_3Ti phase for obtaining Al_3Ti matrix material.

It is inevitable that the porous materials consisting of ductile phase matrix have a

slope in the plateau region because of the strain hardening even when brittle phase is formed. The strain hardening leads to low energy absorption efficiency (Fig. 12 (b)). However, most of the porous intermetallic compounds exhibit serrated or unstable plateau regions with decrement in flow stress [7, 8], resulting in decreasing the energy absorption capacity (Fig. 12 (a)). Porous intermetallic compounds hybridizing with ductile phase do not exhibit the strain hardening due to poor deformability of the brittle matrix and suppress the decrement in the flow stress by arresting crack propagation at the ductile phase. Therefore, hybridization of intermetallic compounds matrix with ductile phase are effective for improving both energy absorption capacity and efficiency of the porous materials although further researches of other systems will be needed.

5. Conclusion

In the present study, the porous Al/Al_3Ti/Ti hybrids with various fraction of brittle Al_3Ti phase were synthesized by reaction sintering with NaCl space holder powder. Effects of sintering temperature and time on porous structure, microstructure and compressive properties were investigated. The area fraction of Al_3Ti phase increased according the Johnson-Mehl-avrami-Koromogrov equation with an exponent of 1.5 although the porous structure formed by NaCl space holder did not change depending on the sintering conditions. The porous Al/Al_3Ti/Ti hybrid with the area fraction of Al_3Ti phase of approximately 70% exhibited a flat plateau region (the slope is approximately zero) with a large plateau end strain (approximately 60%). In the porous Al/Al_3Ti/Ti hybrid, Al_3Ti phase matrix suppressed the strain hardening of cell wall by brittle fracture and Al phase suppressed decrement in the flow stress by arresting the crack propagation. Therefore, porous intermetallic compounds hybridizing with ductile

phase are promising impact energy absorbers.

References

[1] J. Banhart, Manufacture, characterization and application of cellular metals and metal foams, Prog. Mater. Sci. 46 (2001) 559–632. https://doi.org/10.1016/S0079-6425(00)00002-5.

[2] International Organization for Standardization: Metallic materials-Ductility testing-Compression test for porous and cellular metals, ISO 13314 (2011).

[3] K. Kitazono, Design of impact energy absorbing system based on porous aluminum, J. Jpn. Inst. Light Metals, 67 (11) (2017) 559-563.

[4] N. Michailidis, F. Stergioudi, A. Tsouknidas, E. Pavlidou, Compressive response of Al-foams produced via a powder sintering process based on a leachable space-holder material, Mater. Sci. Eng. A 528 (2011) 1662-1667.

[5] M. Hakamada, M. Mabuchi, Fabrication by spacer method and evaluation of porous metals, J. Jpn. Inst. Light Metals, 62 (8) (2012) 313-321.

[6] N. Takata, K. Uematsu, M. Kobashi, Compressive properties of porous Ti-Al alloys fabricated by reaction synthesis using a space holder powder, Mater. Sci. Eng. A 697 (2017) 66-70.

[7] W. Jie, C. Hong-zhi, C. Li-li, G. Zheng-zheng, Open-celled porous NiAl intermetallics prepared by replication of carbamide space-holders, Trans. Nonferrous Met. Soc. China 21 (2011) 1750-1754.

[8] Y. Shu, A. Suzuki, N. Takata, M. Kobashi, Microstructure and Mechanical property of Porous Nickel aluminides Fabricated by Reactive Synthesis with Space Holder Powder, MRS advances, in press.

[9] T. Ikeda, M. Tsukamoto, H. Nakajima, Fabrication of lotus-type porous stainless steel by unidirectional solidification under hydrogen atmosphere, Mater. Trans. 43 (2002) 2678–2684. https://doi.org/10.2320/matertrans.43.2678.

[10] S.-K. Hyun, T. Ikeda, H. Nakajima, Fabrication of lotus-type porous iron and its mechanical properties, Sci. Technol. Adv. Mater. 5 (2004) 201–205. https://doi.org/10.1016/j.stam.2003.11.005.

[11] T. Shimizu, K. Matsuzaki, Processing technology for high porosity closed cell metal foam, Por. Met. Met. Foam. Technol. (2005) 191–194.

[12] S. Angel, W. Bleck, P.F. Scholz, T. Fend, Influence of powder morphology and chemical composition on metallic foams produced by slip reaction foam sintering (SRFS) process, Steel Res. Int. 75 (2004) 483–488. https://doi.org/10.1002/srin.200405800.

[13] Y.Y. Zhao, D.X. Sun, A novel sintering–dissolution process for manufacturing Al foams, Scripta Mater. 44 (2001) 105–110.

[14] A. Ibrahim, C. Körner, R.F. Singer, The effect of TiH2 particle size on the morphology of Al-foam produced by PM process, Adv. Eng. Mater. 10 (2008) 845–848.

[15] A.R. Kennedy, S. Adavavisithchai, Foaming of compacted Al-TiH2 powder mixtures, Mater. Sci. Forum 396–402 (2002) 251–258. https://doi.org/10.1002/adem.200800139.

[16] M. Kobashi, N. Kanetake, Processing of intermetallic foam by combustion reaction, Adv. Eng. Mater. 4 (2002) 745–747. https://doi.org/10.1002/1527-2648(20021014)4:10<745::AID-ADEM745>3.0.CO;2-U.

[17] Y. Arakawa, M. Kobashi, N. Kanetake, Foaming behavior of long-scale Al–Ti intermetallic foam by SHS mode combustion reaction, Intermetallics 41 (2013) 22–27. https://doi.org/10.1016/j.intermet.2013.04.004.

[18] K. Morsi. Review: reaction synthesis processing of Ni–Al intermetallic materials, Mater. Sci. Eng. A 299 (2001) 1–15.

[19] H.C. Yi, J.J. Moore, Self-propagating high-temperature (combustion) synthesis (SHS) of powder-compacted materials, J. Mater. Sci. 25 (1990) 1159–1168.

[20] H. Ran, J. Niu, B. Song, X. Wang, P. Feng, J. Wang, Y. Ge, A. Farid, Microstructure and properties of Ti5Si3-based porous intermetallic compounds fabricated via combustion synthesis J. Alloys Compd. 612 (2014) 337-342.

[21] M. Kobashi, S. Miyake, N. Kanetake, Hierarchical open cellular porous TiAl manufactured by space holder process Intermetallics 42 (2013) 32–34.

[22] X. Jiao, X. Wang, X. Kang, P. Feng, L. Zhang, J. Wang, F. Akhta, Hierarchical porous TiAl3 intermetallics synthesized by thermal explosion with a leachable space-holder material Mater. Lett. 181 (2016) 261–264.

[23] Y. Shu, A. Suzuki, N. Takata, M. Kobashi, Fabrication of porous NiAl intermetallic compounds with a hierarchical open-cell structure by combustion synthesis reaction and space holder method, J. Materials. Processing Tech. 264 (2019) 182-189.

[24] H. Feng, D. Jia, Y. Zhou, Spark plasma sintering reaction synthesized TiB reinforced titanium matrix composites, Composites: Part A 36 (2005) 558-563.

[25] J. C. Schuster and M. Palm, Reassessment of the Binary Aluminum-Titanium Phase Diagram, J. Phase Equilibria and Diffusion 27(3) (2006) 255-277.

[26] A. Suzuki, Y. Arai, N. Takata, M. Kobashi, Structural design and bonding strength evaluation of Al/epoxy resin joint via interpenetrating phase layer, Journal of Materials Processing Tech. 262 (2018) 11–18.

[27] A. N. Kolmogorov, On the statistical theory of the crystallization of metals, Bull. Acad. Sci. USSR, 3 (1937) 355.

[28] M. Avrami, Kinetics of Phase Change. II Transformation-Time Relations for Random Distribution of Nuclei, J. Chem. Phys. 8 (1940) 212.

[29] W. A. Johnson and R. F. Mehl, Trans, AIME 135, (1939) 416.

[30] J.W. Christian, Phase Transformations, Physical Metallurgy edited by R. W. Cahn, North-Holland Publishing Company-Amsterdam Chap. 10 (1965) 471-587.

[31] N. Jha, D.P. Mondal, J. D. Majumdar, A. Badkul, A.K. Jha, A.K. Khare, Highly porous open cell Ti-foam using NaCl as temporary space holder through powder metallurgy route, Materials and Design 47 (2013) 810–819.

[32] A. Mansourighasri, N. Muhamad, A.B. Sulong, Processing titanium foams using tapioca starch as a space holder, Journal of Materials Processing Technology 212 (2012) 83– 89.

[33] M. Mirjalili, M. Soltanieh, K. Matsuura, M. Ohno, On the kinetics of $TiAl_3$ intermetallic layer formation in the titanium and aluminum diffusion couple, Intermetallics 32 (2013) 297-302.

[34] DJ. Goda, NL. Richards, WF. Caley, MC. Chaturvedi, The effect of processing variables on the structure and chemistry of Ti-aluminide based LMCS, Mater. Sci. Eng. A 334 (2002) 280-290.

[35] FJJ. van Loo, GD. Rieck, Diffusion in the titanium-aluminium system-I. Interdiffusion between solid Al and Ti or Ti-Al alloys. Acta Metall. 21 (1973) 61-71.

[36] K.N. Kulkarni, Y. Sun, A.K. Sachdev, E. Lavernia, Field-activated sintering of blended elemental γ-TiAl powder compacts: Porosity analysis and growth kinetics of Al_3Ti, Scripta Materialia 68 (2013) 841–844.

[37] M. Yamaguchi, F. Nakamura, Y. Shirai, Plasticity of Al_3Ti and possibility of its being improved, J. Jpn. Inst. Light Metals, 38 (4) (1988) 228-237.